CALPHAD: Computer Coupling of Phase Diagrams and Thermochemistry 38 (2012) 23–34

Contents lists available at SciVerse ScienceDirect

CALPHAD: Computer Coupling of Phase Diagrams and Thermochemistry

journal homepage: www.elsevier.com/locate/calphad

Thermodynamic study and re-assessment of the Ge-Ni system

Shan Jin [a,b,*], Christian Leinenbach [a], Jiang Wang [a], Liliana I. Duarte [a], Simona Delsante [c], Gabriella Borzone [c], Andrew Scott [d], Andrew Watson [d]

[a] EMPA, Swiss Federal Laboratories for Materials Science and Technology, Laboratory for Joining and Interface Technology, Überlandstrasse 129, CH-8600 Dübendorf, Switzerland
[b] Computational Materials Laboratory, Ecole Polytechnique Fédérale de Lausanne, Station 12, CH-1015 Lausanne, Switzerland
[c] Department of Chemistry and Industrial Chemistry, University of Genova, Italy
[d] Institute for Materials Research, SPEME, University of Leeds, LS2 9JT, UK

ARTICLE INFO

Article history:
Received 21 December 2011
Received in revised form
13 March 2012
Accepted 17 March 2012
Available online 8 May 2012

Keywords:
Ge-Ni system
Thermodynamic
First-principles calculations
Calorimetry
CALPHAD

ABSTRACT

The enthalpies of formation of the intermetallic compounds in the Ge-Ni binary system have been determined by calorimetric measurement and first-principles calculations. Based on the results obtained and information available in the literature, the phase diagram and thermodynamic properties of the Ge-Ni system have been re-assessed using the CALPHAD approach [L. Kaufman, H. Bernstein, Computer Calculation of Phase Diagrams, Academic Press, New York (1970)], applying appropriate thermodynamic models for the phases. The liquid phase and the Ni-based solid solution (Ni) were modeled as substitutional solutions using the Redlich-Kister equation to represent the excess Gibbs energy. The *B*8-type intermediate phases εNi_5Ge_3, $Ni_{19}Ge_{12}$ and Ni_3Ge_2 were treated as a single phase, designated as Ni_5Ge_3. A three-sublattice model with stoichiometry (Ge)(Ni)(Va,Ni) was used to describe the *B*8-type Ni_5Ge_3-phase based on its crystal structure. The order-disorder transformation between disordered FCC_A1 and the ordered $L1_2$-type phase, βNi_3Ge, was treated using a two-sublattice model. The other five intermetallic compounds were treated as stoichiometric compounds. The phase diagram and the thermodynamic properties calculated from the optimized model parameters are in good agreement with most of the experimental data.

1. Introduction

The increasing pressure to eliminate lead from electronic devices has stimulated great interest in the search for lead-free solders. Au-Ge based alloys are promising high-temperature lead-free solders because of their low melting temperature, high conductivity, good glass forming ability and excellent corrosion resistance [1,2]. Moreover, the good wettability of Au-Ge eutectic alloys on Cu and Ni substrates has been reported recently [3].

In addition, as an important semiconductor material, Ge has been considered as a replacement for Si-channels in future high-speed complementary metal oxide semiconductor (CMOS) technology because of its higher intrinsic mobility [4]. With low formation temperatures and low resistivities, nickel germanides are promising candidates as contact materials for Ge-channel devices [5]. Moreover, a eutectic (28 at% Ge) Au-Ge alloy with a Ni layer is used widely in the fabrication of ohmic contacts in n-type GaAs [6,7].

In both the electronic packaging and semiconductor industry areas mentioned above, knowledge of phase equilibria and thermodynamic stabilities of the phases is crucial, e.g., the reliability of solder joints is strongly dependent on the phases formed at the solder/substrate interface. Therefore, considering the many prospective applications of the Au-Ge-Ni alloy system, thermodynamic modeling of the Au-Ge-Ni ternary system is important. As a first step, the present work is focused on a thermodynamic study of the Ge-Ni binary system.

The phase diagram and thermodynamic properties of the Ge-Ni system have been investigated extensively. Nevertheless, there are still some uncertainties, especially with regard to the enthalpies of formation of the intermetallic compounds. Values reported in the literature are incompatible with each other [8,9].

A thermodynamic assessment of the Ge-Ni binary system has been carried out by Liu et al. [10]. Their calculated results reproduce well most of the available experiment data in the literature. However, for simplicity, Liu et al. [10] only considered the homogeneity ranges when choosing the sublattice model for describing the intermetallic compounds (βNi_3Ge, εNi_5Ge_3, $Ni_{19}Ge_{12}$ and Ni_3Ge_2 have considerable ranges of homogeneity),

* Corresponding author at: EMPA, Swiss Federal Laboratories for Materials Science and Technology, Laboratory for Joining and Interface Technology, Überlandstrasse 129, CH-8600 Dübendorf, Switzerland. Tel.: +41 44 823 4825; fax: +41 58 765 1122.
E-mail address: shan.jin@empa.ch (S. Jin).

0364-5916/$ - see front matter © 2012 Elsevier Ltd. All rights reserved.
http://dx.doi.org/10.1016/j.calphad.2012.03.003

while the crystal structures themselves were not taken into account. The development of a consistent thermodynamic database requires the unification of the models for phases with the same type of crystal structure.

Therefore, the purposes of the present work are, (i) to determine the enthalpies of formation of the intermetallic compounds through first-principles calculations and calorimetric measurement, (ii) to provide a consistent and reliable thermodynamic description of the Ge-Ni binary system using the CALPHAD (CALculation of PHAse Diagram) method [11].

2. Evaluation of the experimental information from the literature

2.1. Phase diagram information

The Ge-Ni phase diagram has been studied experimentally by several groups [12–14]. The first comparatively complete Ge-Ni phase diagram was proposed by Ruttewit and Masing [12] following a thermal analysis study. Later, Dayer and Feschotte [13] reinvestigated the Ge-Ni phase diagram in detail through differential thermal analysis, X-ray diffraction, micrography, microhardness and X-ray microprobe analysis. In the intervening years, Ellner et al. [14] studied the region between 25 and 50 at% Ge. The phase diagram data from Dayer and Feschotte [13] were given preference during the present optimization because of the higher purity of starting materials (99.999% Ge and 99.99% Ni) used.

There are 9 intermetallic compounds, namely βNi_3Ge, γNi_3Ge, δNi_5Ge_2, Ni_2Ge, εNi_5Ge_3, $Ni_{19}Ge_{12}$, Ni_3Ge_2, $\varepsilon' Ni_5Ge_3$ and NiGe, in the currently accepted Ge-Ni phase diagram, which was evaluated by Nash et al. [15]. Among these, βNi_3Ge is reported as having an ordered cubic structure by Pfisterer and Schubert [16], and this was later confirmed by Lecocq [17] and Ellner et al. [14], who found that βNi_3Ge has the ordered variant of the disordered FCC_A1 structure ($L1_2$-type). It melts congruently at 1405 K, according to [13]. The homogeneity range of βNi_3Ge was determined by [13] to be 22.5 to 25 at% Ge over the whole temperature range, while later investigation [18] using electron probe microanalysis (EPMA) shows a reduction in the homogeneity range with decreasing temperature. Using analytical electron microscopy (AEM) and EPMA, Komai et al. [19] measured the compositional variations across a Ni/βNi_3Ge diffusion couple interface and supported the trend observed in [18]. Therefore, the homogeneity range of βNi_3Ge measured by Ikeda et al. [18] was given more weight in the present optimization.

The homogeneity range of the $B8$ phase is from 33 to 45 at% Ge. Ruttewit et al. [12], Gel'd et al. [20] and Dayer et al. [13] considered this region to be a wide non-stoichiometric Ni_5Ge_3 solid solution. However, the existence of three separate phases, εNi_5Ge_3, $Ni_{19}Ge_{12}$ and Ni_3Ge_2 instead of one phase in this region was reported by Ellner et al. [14] and later confirmed by Larsson et al. [21]. εNi_5Ge_3 and Ni_3Ge_2 were given as disordered $B8_1$ phases and $Ni_{19}Ge_{12}$, which lies between εNi_5Ge_3 and Ni_3Ge_2, was reported to exhibit a commensurate superstructure of an underlying $B8$ type sub-structure [14,21]. This region in the currently accepted Ge-Ni phase diagram [15] is based on the work of Ellner et al. [14]. The phase boundaries of the εNi_5Ge_3, $Ni_{19}Ge_{12}$ and Ni_3Ge_2 phases were investigated by Ellner et al. [14] using thermal analysis, Dayer et al. [13] using microprobe, and more recently, by Ikeda et al. [18] using EPMA. All of these phase boundary data were taken into account during the present optimization.

The γNi_3Ge, δNi_5Ge_2, Ni_2Ge, $\varepsilon' Ni_5Ge_3$ (low-temperature form of εNi_5Ge_3) and NiGe phases are formed by peritectic or peritectoid reactions, and each of them has no or a rather narrow homogeneity range.

The maximum solid solubility of Ge in (Ni) was reported to be about 16 at% Ge at 1124 °C by Dayer et al. [13] and 12 at% Ge at 1157°C by Ruttewit et al. [12], respectively. In addition, Lecocq [17] measured the solid solubility of Ge in (Ni) to be 13 at% Ge at 800 °C based on Curie temperature measurement. Dayer et al. [13] measured the solubility of Ge in (Ni) between 700 °C and 1000° C. Brahman et al. [22] determined the solubility of Ge in (Ni) using lattice parameters measurement and chemical analysis by SEM and their results were internally consistent with the microprobe results of Dayer et al. [13]. Ikeda et al. [18] and Komai et al. [19] determined the phase boundary compositions of the phase equilibria between (Ni) and βNi_3Ge. Both results are in good agreement with those of Dayer et al. [13].

The solubility of Ni in (Ge) is negligible and was not considered in the present work.

Ellner et al. [12] elucidated the crystal structures of all phases in the Ge-Ni system and they are listed in Table 1.

The Curie temperature was measured as a function of composition by Lecocq [17] (0–300 °C) and Ilonca [23] (−150 to 0 °C). The data covered different temperature ranges but agree where they overlap.

2.2. Thermodynamic properties

The enthalpies of mixing of Ge-Ni melts have been determined at different temperatures [24–29]. Using a high-temperature Calvet-calorimeter and the drop method, Castanet [24] measured

Table 1
Enthalpies of formation of intermetallic compounds in the Ge-Ni binary system obtained from first-principles calculations and calorimetric experiments in the present work.

Phase	Pearson symbol/Space group/ Strukturbericht designation/Structure type	Composition, at.% Ge	T_{ref}, K	$\Delta_f H$ (T_{ref}), kJ/mol	Method
βNi_3Ge	$cP4/Pm\bar{3}m/L1_2/Cu_3Au$	25	1063	−35.0	Calorimetry
		–	Ground state	−31.6	DFT
δNi_5Ge_2	$hP84/P6_3/mmc$/-/Pd_5Sb_2	–	Ground state	−30.3	DFT
Ni_2Ge	$oP12/Pnma/C23/Co_2Si$	–	Ground state	−33.1	DFT
εNi_5Ge_3 (Ni_5Ge_3)	$hP6/P6_3/mmc/B8_1$/NiAs	36	1063	−37.0	Calorimetry
$\varepsilon' Ni_5Ge_3$	$mC32/C2/-/Ni_5Ge_3$	–	Ground state	−33.8	DFT
$Ni_{19}Ge_{12}$ (Ni_5Ge_3)	$mC62/C2/-/Ni_{19}Ge_{12}$	–	Ground state	~−32.5	DFT
Ni_3Ge_2 (Ni_5Ge_3)	$hP6/P6_3/mmc/B8_1$/NiAs	44	1063	−34.0	Calorimetry
NiGe	$oP8/Pnma/B31$/MnP	50	1033	−30.0	Calorimetry
		–	0	−34.9	DFT

the enthalpies of mixing of liquid Ge-Ni alloys at 1288 K in the range of 48.26 to 93.63 at% Ge. Shlapak et al. [25] measured the heats of formation of molten Ge-Ni alloys at 1773 K from 8.8 to 83.5 at% Ge using solution calorimetry. Esin et al. [26] calorimetrically determined the enthalpies of Ge-Ni melts at the same temperature as Shlapak et al. [25], 1773 K, but more exothermic values have been obtained. Kant [27] derived the heat of formation of liquid $Ni_{0.6}Ge_{0.4}$ alloys from activity measurements made using Knudsen effusion coupled with mass spectroscopy. They gave a wide range of values, from −25100 to −62760 J/mol. Recently, the integral enthalpy of mixing of Ge-Ni melts at 1800 K was deduced by the Darken method using the partial enthalpy of mixing of Ni in Ge-Ni melts [28] measured calorimetrically. The enthalpies of mixing of Ge-Ni melts were also derived from activities measured using Knudsen Cell effusion for temperatures from 1640 to 1920 K [29] but the values are less exothermic than other studies. Note that the uncertainty of indirect methods is large. The enthalpies of mixing of Ge-Ni melts measured by Castanet [24] are more exothermic than other studies, which might be due to the lower measuring temperature (1288 K). The enthalpies of mixing determined by Sudavtsova et al. [28] at 1800 K agree well with those determined by Esin et al. [26] at 1733 K, while both of them are more exothermic than those measured by Shlapak et al. [25] at 1773 K. Therefore, preference was given to the values determined by Castanet [24] at 1288 K, Esin et al. [26] at 1773 K and Sudavtsova et al. [28] at 1800 K during the optimization.

The partial enthalpy of mixing of Ni in Ge-Ni melts at 1800 K was measured using high-temperature isoperibol calorimetry by Sudavtsova et al. [28] in the composition range $0 < x_{Ni} < 0.7$ ($\Delta_{mix}\overline{H}^{\infty}(\mathrm{Ni}) = -76.0 \pm 4.8$ kJ/mol). The partial enthalpies of mixing of Ge were then evaluated from $\Delta_{mix}\overline{H}(\mathrm{Ni})$. Castanet [30] measured the partial molar enthalpy of mixing of Ni in liquid Ge at 1274 K to be −78.3 kJ/mol using high temperature calorimetry. Esin et al. [26] measured the partial enthalpy of Ge and Ni in Ge-Ni melts at 1773 K. Shlapak et al. [25] calculated $\Delta_{mix}\overline{H}(i)$ from the measured heats of mixing of Ge-Ni liquid alloys. The $\Delta_{mix}\overline{H}(\mathrm{Ni})$ measured by Sudavtsova et al. [28] are considered to be more reliable since the data measured by Esin et al. [26] have a complex shape in the Ge-rich region, which is inconsistent with the Ge-Ni phase diagram. The $\Delta_{mix}\overline{H}(\mathrm{Ge})$ data determined by Esin et al. [26] were given more weight during the optimization since the values reported by Sudavtsova et al. [28] and Shlapak et al. [25] were obtained by calculation.

Using Knudsen cell mass spectrometry, Erdélyi et al. [29], Kant [27] and Berezuts′kyi et al. [31] determined the activities of Ge and Ni in Ge-Ni melts in the temperature ranges 1640–1920 K, 1700–1800 K and 1623 K, respectively. Sudavtsova et al. [28] evaluated the Ge activity at 1750 K from the liquidus coordinates in the Ge-Ni phase diagram using the Schroeder equation [32] and a modified Hauffe-Wagner method [33]. The results of Sudavtsova et al. [28] agree well with the data reported by Erdélyi et al. [29]. Thus, activities determined by Erdélyi et al. [29] are considered to be more reliable and so were used during the optimization.

The excess and partial Gibbs energies of mixing and excess entropies of mixing were determined using Knudsen cell-mass spectrometry in the temperature range 1640 to 1920 K by Erdélyi et al. [29]. Batalin and Shlapak [34] calculated partial and integral free energies and entropies of mixing of liquid Ge-Ni alloys from phase equilibrium data [35] and data from Shlapak et al. [25] using the Kubaschewski-Chart equation [36]. By applying the method of determining thermodynamic coefficients, which was developed for solid solutions, to liquid Ge-Ni alloys, Erokhin and Gurov [37] calculated the total, excess, and partial molar Gibbs energies and the total and excess entropies of liquid Ge-Ni alloys at 1773 K. Sudavtsova et al. [28] calculated the thermodynamic properties of Ge-Ni melts at 1870 K, including total and partial Gibbs energies of mixing, total and partial entropies of mixing and excess entropies of mixing.

The activities of Ge in solid Ge-Ni alloys were determined in the temperature range from 950 to 1100 K and the concentration range $x_{Ge} = 0.240$–0.447 by electromotive force (EMF) measurement [38]. The molar heat capacity of NiGe was determined using differential scanning calorimetry over the temperature range 310–1080 K by Perring et al. [39]. No heat capacity information for the other intermetallic compounds has been reported up to now.

The enthalpies of formation of solid alloys at 330 K and 1060 K were determined using tin solution calorimetry by Martosudirjo et al. [8] and Predel et al. [9], respectively. The enthalpy of formation of εNi_5Ge_3 was determined by Kleppa et al. [40] and Predel et al. [41] using calorimetry. The value obtained by Kleppa et al. [40] is in good agreement with the enthalpy of formation of εNi_5Ge_3 measured by Martosudirjo et al. [8] and Predel et al. [9] while Predel et al. [41] reported more exothermic values. However, the enthalpy of formation reported by Martosudirjo et al. [8] and Predel et al. [9] are incompatible with each other both in the value and trend.

3. Determination of enthalpy of formation of the intermetallic compounds

Considering the incompatibility of the enthalpies of formation of the solid alloys reported in the literature [8,9], the enthalpies of formation of the intermetallic compounds in the Ge-Ni system have been determined by first-principles calculations and calorimetric measurement in the present work.

3.1. First-principles calculations

Ab-initio calculations of the zero temperature enthalpy of formation (total energy) were performed using the plane wave, pseudopotential, density functional theory (DFT) code, CASTEP [42]. Exchange-correlation was treated using the PBE formalism of the generalized gradient approximation [43] with the use of ultra-soft pseudopotentials. A kinetic energy cut-off of 500 eV and a k-point sampling distance of ~ 0.2 Å^{-1} were used. These parameters having been chosen to give energy precisions of better than 0.5 kJ mol^{-1}. Spin was unrestricted, this being important for the geometry optimization and energy determination of the ferromagnetic Ni structure. For consistency, all the element and compound structures were geometry optimized with a force tolerance of 0.01 eVÅ^{-1}. Compound enthalpies were referenced to Ni (*Fm*-3*m*) and Ge (*Fd*-3*m*).

Table 1 lists the compound enthalpies obtained from first-principles calculations.

3.2. Calorimetric measurements

3.2.1. Experimental procedure

The calorimetric samples have been prepared by weighing, in a glove box, appropriate amounts of Ni (−120 mesh, Alfa Aesar, Puratronic®, (metal basis) 99.996 % - C typically < 0.05 %) and Ge (−100 mesh, Alfa Aesar, (metal basis) 99.999 %) powders which were then mixed and pressed to obtain pellets of about 8 mm diameter and 4 mm in height. Eighteen samples have been prepared with compositions in the range 24–51 at% Ge.

Calorimetric measurements were performed using a high-temperature drop calorimeter, built in-house, the details of which have been given elsewhere [44,45]. It consists of a receiving vessel held at the selected high temperature (T_c). A reference

sample is contained in the same region of the furnace, together with a sensor comprising a thermopile (20 thermocouples) differentially connected to the reference sample and to the receiving vessel. For the measurement, the pelleted samples were sealed in tantalum crucibles and dropped into the calorimeter from a thermostatically controlled chamber (at $T=T_0=300$ K) standing directly above the receiving vessel.

For each measurement, the EMF of the thermopile is sampled by a data acquisition system every 4 s, starting 600 s before the drop and continuing for up to about 4000 s. The signal resulting from the heat change within the receiving vessel is much reduced and within zero fluctuation generally after 1000 s. The acquisition system computes the integral of the difference between the signal and the base line. The heat effect is evaluated through a series of calibration runs performed by dropping specimens of known heat content (typically pieces of pure silver weighting 1.0–1.5 g) into the calorimeter and recording the signal associated with the heat change. The measurement temperature of the calorimeter T_c, was set at 1033 K or 1063 K considering the shape of the phase diagram and the composition of the samples. Some details are given below.

During the measurement, the total heat effect Q is due to the heat of the reaction:

$$x\mathrm{Ge}(\mathrm{cr},T_c)+(1-x)\mathrm{Ni}(\mathrm{cr},T_c)\rightarrow \mathrm{Ge}_x\mathrm{Ni}_{(1-x)}(\mathrm{cr},T_c),\quad \text{at temperature } T_c, \tag{1}$$

plus that relating to the enthalpy increment of Ge, Ni and of the tantalum crucible.

Therefore, Q for 1 mol of $Ge_xNi_{(1-x)}$ alloy (enclosed in the Ta crucible, atomic weight 180.95, having a mass m_{cruc}) is:

$$Q = x(H_{Tc}-H_{T0})(\mathrm{Ge},\mathrm{cr})+(1-x)(H_{Tc}-H_{T0})(\mathrm{Ni},\mathrm{cr}) + m_{\mathrm{cruc}}(H_{Tc}-H_{T0})(\mathrm{Ta},\mathrm{cruc})/180.95+\Delta_f H(\mathrm{Ge}_x\mathrm{Ni}_{(1-x)},\mathrm{cr},T_c) \tag{2}$$

By using the Dinsdale's polynomial expression [46] for the specific heat for Ge, Ni and Ta over the appropriate temperature range, the enthalpy increments between T_0 and T_c have been calculated in order to obtain the value of $\Delta_f H$ of the alloy at T_c.

The measurement uncertainty limits are estimated to be $\pm(0.3–0.5)$ kJ/mol in any run. Nevertheless, the accuracy of calorimetric measurements is related to the actual processes occurring in the calorimeter. The sensitivity of the calorimeter was obtained by dropping, under different conditions of mass and temperature, several samples of known heat content as a function of the total mass accumulated in the measuring cell. Further tests carried out by dropping Ag samples of different masses into the calorimeter at 973 K showed that the sensitivity is independent of the size of heat effect in the energy range between 50 and 1000 J.

To make an overall evaluation, the completeness of the synthesis reaction, the attainment of the equilibrium state, the presence/absence of side reactions, etc. should be considered. To this end, the composition and state of the samples were verified by means of microscopic (optical and electron probe microanalysis) and X-ray diffraction analysis after the calorimetric measurements.

Firstly, the microstructure of the alloys was observed using a Leica DM4000 M optical microscope equipped with a Leica DFC Camera and X-Plus Alexasoft software. Subsequently, a thorough investigation of each sample was completed using a Scanning Electron Microscope (Zeiss-EVO 40). The compositional contrast between the different phases was obtained using a backscattered electron (BSE) detector, and quantitative data were collected at 20 kV on a *Link system Ltd.* instrument, equipped with an Energy-Dispersive Spectroscopy (EDS) detector. A counting time of 100 s and a ZAF correction program were used. Certified pure elements were used as reference standards, while cobalt was adopted for calibration purposes. The software package Inca Energy (Oxford Instruments, Analytical Ltd., Bucks, U.K.) was employed to process the X-ray spectra.

Powder X-ray diffraction (XRD) was performed using a Philips *X'Pert MPD* machine (Philips, Almeno, The Netherlands) equipped with a copper target, excited to 40 kV and 30 mA, and a solid state detector.

3.2.2. Results

Following the calorimetric measurement, the synthesized samples were brittle and often showed a degree of porosity. Microscopy examinations confirmed that no reaction occurred with the Ta crucibles during the calorimetric synthesis of the Ni-Ge samples. After the XRD and SEM/EDS characterization, the enthalpy values of the samples which had not reached thermodynamic equilibrium were rejected.

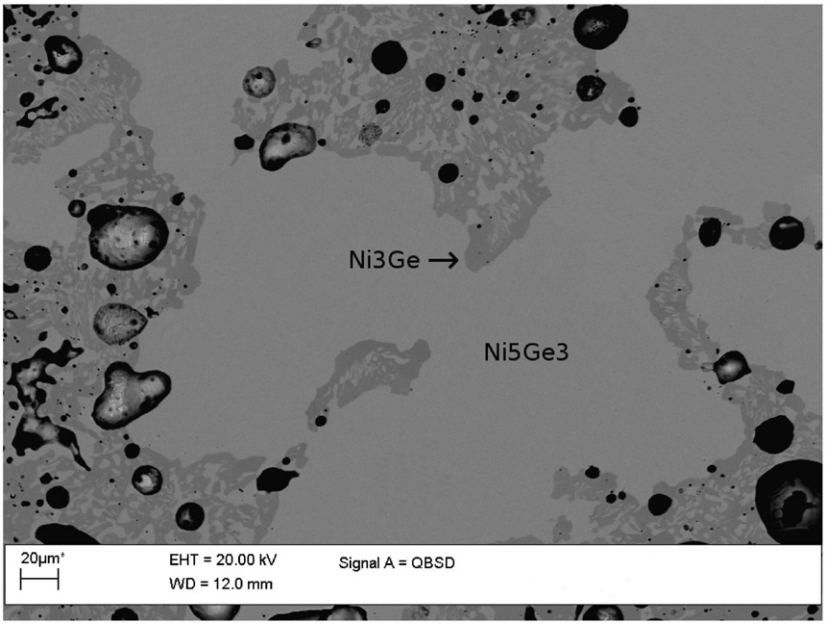

Fig. 1. SEM micrograph (BSE signal), after calorimetric measurement at $T_c=1063$ K, of the Ni-Ge (30 at% Ge) sample; light grey phase: Ni_5Ge_3 with composition $\sim Ni_{64}Ge_{36}$; grey phase: βNi_3Ge with composition $\sim Ni_{75}Ge_{25}$. Porosity visible.

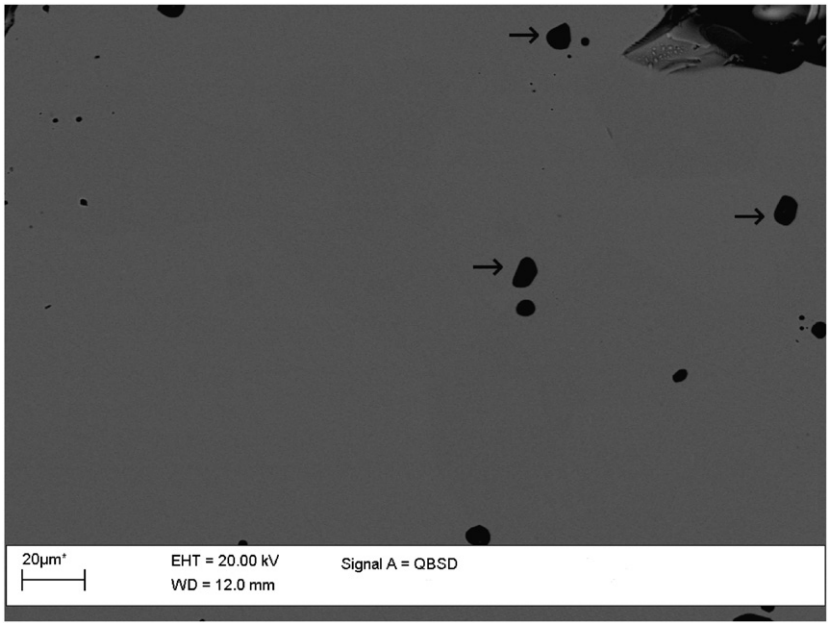

Fig. 2. SEM micrograph (BSE signal), after calorimetric measurement $T_c = 1033$ K, of the Ni-Ge (41 at% Ge) sample; the only phase detected is Ni_5Ge_3. Holes are indicated by arrows.

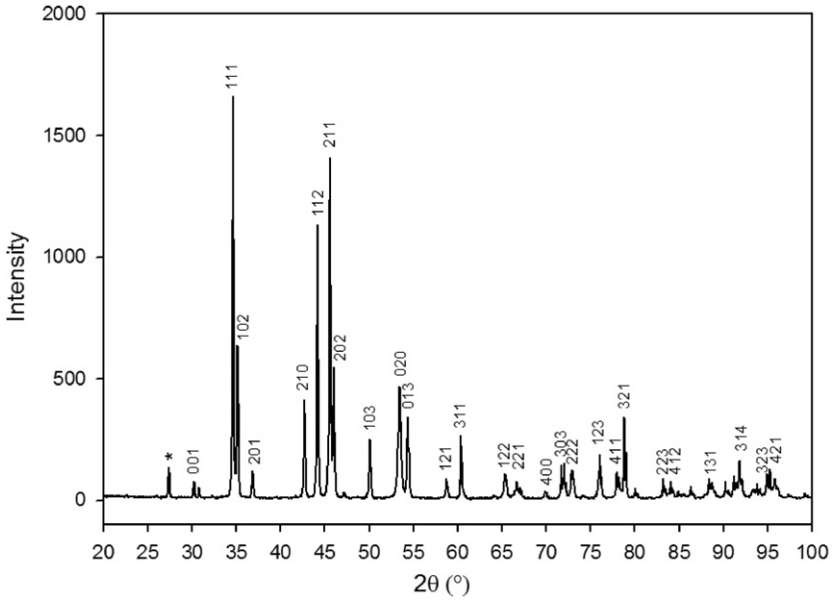

Fig. 3. Diffraction pattern, after calorimetric measurement, of the Ni-Ge (51 at% Ge) sample: the indexed peaks belong to the orthorhombic (o*P*8) GeNi phase. The peak with a $2\theta \approx 27^\circ$, indicated with the asterisk, belongs to pure Ge (c*F*8).

In Fig. 1 is shown the SEM image (back-scattered signal - BSE) of the sample having the composition Ni-Ge (30 at% Ge) in which the βNi_3Ge phase and the Ni_5Ge_3 phase can be seen. Porosity and holes are also present. The SEM image (BSE signal) of the single-phase sample Ni-Ge (41 at% Ge) is shown in Fig. 2; as in the previous case, some holes are observed.

The XRD analysis of the calorimetric samples with composition in the range 36 - 44 at% Ge, showed the presence of the hexagonal phase (*hP*6); the orthorhombic structure (o*P*8) of the NiGe phase and the cubic structure (*cP*4) of the βNi_3Ge phase are also confirmed. Fig. 3 shows the diffraction pattern of the Ni-Ge (51 at% Ge) sample: all peaks belong to the orthorhombic (o*P*8) NiGe phase (almost all *hkl* values are also inserted) except the one with a 2θ value of around 27°, indicated with the asterisk, which belongs to pure Ge. The values obtained for the enthalpies of formation at T_c for the cubic βNi_3Ge, for the hexagonal Ni_5Ge_3 (at the limiting compositions) and the orthorhombic NiGe phases are given in Table 1. The reference states for the data are the solid components (Ge c*F*8-C type and Ni c*F*4-Cu type). The most exothermic value of the enthalpy of formation occurs at a composition of 36 at% Ge.

4. Thermodynamic modeling

4.1. Pure elements

The pure elements in their stable structures at 298.15 K and 1 bar are chosen as the reference states for the system. The thermodynamic functions of the pure elements in their stable and

metastable states are taken from the Scientific Group Thermodata Europe (SGTE) database [46] and are described as:

$$^{0}G_i^{\varphi}(T) = G_i^{\varphi}(T) - H_i^{SER} = a + bT + cT\ln T + dT^2 + eT^3 + fT^{-1} + gT^7 + hT^{-9} \quad (3)$$

where H_i^{SER} is the molar enthalpy of the element i (i=Ge or Ni) at 298.15 K and 1 bar in its standard element reference (SER) state; T is the absolute temperature; $G_i^{\varphi}(T)$ is the absolute molar Gibbs energy of the element i with structure of φ; $^{0}G_i^{\varphi}(T)$ is the molar Gibbs energy of the element i with the structure of φ referred to the enthalpy of its stable state at 298.15 K and 1 bar.

4.2. Solution phases

The substitutional solution model was employed to describe the solution phases (Liquid, FCC_A1 and DIAMOND_A4) in this system. The molar Gibbs energy of the solution phase φ (φ=Liquid, FCC_A1 and DIAMOND_A4) can be expressed as:

$$G_m^{\varphi} = \sum x_i\,^{0}G_i^{\varphi} + RT\sum x_i\ln(x_i) + {}^{E}G_m^{\varphi} + {}^{mag}G_m^{\varphi} \quad (4)$$

where G_m^{φ} is the molar Gibbs energy of a solution phase φ; $^{0}G_i^{\varphi}$ is the molar Gibbs energy of the element i (i=Ge or Ni) with the structure φ in a nonmagnetic state; x_i the mole fraction of component i, R gas constant, T temperature; $^{E}G_m^{\varphi}$ the excess Gibbs energy, and $^{mag}G_m^{\varphi}$ is the magnetic contribution to the Gibbs energy. The excess Gibbs energy of phase φ can be expressed by the Redlich-Kister polynomial [47] as:

$${}^{E}G_m^{\varphi} = x_{Ge}x_{Ni}\sum_{j=0}^{n} {}^{(j)}L_{Ge,Ni}^{\varphi}(x_{Ge}-x_{Ni})^j \quad (5)$$

Here $^{(j)}L_{Ge,Ni}^{\varphi}$ is the interaction parameter between the elements Ge and Ni and is formulated as temperature dependent:

$${}^{(j)}L_{Ge,Ni}^{\varphi} = A_j + B_jT + C_jT\ln T \quad (6)$$

where A_j, B_j and C_j are model parameters to be optimized in this work.

The magnetic contribution in this system was considered only for the FCC_A1 phase. It was modeled according to the work of Hillert and Jarl [48]:

$${}^{mag}G_m^{\varphi} = RT\ln(\beta^{\varphi}+1)f(\tau^{\varphi}) \quad (7)$$

where τ^{φ} is defined as T/T_c^{φ} with T_c^{φ} being the critical temperature for magnetic ordering; β^{φ} is a quantity related to the total magnetic entropy and is equal to the Bohr magnetic moment per mole of atoms in most cases; $f(\tau^{\varphi})$ represents the polynomials suggested by Hillert and Jarl [48].

The parameters T_c^{φ} and β^{φ} are described by the following expressions:

$$T_c^{\varphi} = x_{Ge}\,^{0}T_{c,Ge}^{\varphi} + x_{Ni}\,^{0}T_{c,Ni}^{\varphi} + x_{Ge}x_{Ni}\sum_{i=0}^{n} T_c^i(x_{Ge}-x_{Ni})^i \quad (8)$$

$$\beta_{\varphi} = x_{Ge}\,^{0}\beta_{Ge}^{\varphi} + x_{Ni}\,^{0}\beta_{Ni}^{\varphi} + x_{Ge}x_{Ni}\sum_{i=0}^{n} \beta^i(x_{Ge}-x_{Ni})^i \quad (9)$$

where $^{0}T_{c,Ge}^{\varphi}$, $^{0}T_{c,Ni}^{\varphi}$, $^{0}\beta_{Ge}^{\varphi}$, $^{0}\beta_{Ni}^{\varphi}$ are the Curie temperature and Bohr magnetons of the pure elements Ge and Ni, respectively. T_c^i and β_i are the magnetic interaction parameters to be assessed in the present work.

4.3. Ordered phase βNi_3Ge

The ordered βNi_3Ge phase with $L1_2$ structure was modeled as $(Ge,Ni)_{0.75}(Ge,Ni)_{0.25}$. In order to represent the Gibbs energy of the order/disorder transition using a single function while allowing the disordered phase to be optimized independently, an approach developed by Ansara and Dupin [49], which has been implemented into the Thermo-Calc software package by Sundman et al. [50], was used. This is done by resolving the compound Gibbs energy into three terms:

$$G_m = G_m^{disord}(x_i) + G_m^{ord}(y_i', y_i'') - G_m^{ord}(x_i) \quad (10)$$

where $G_m^{disord}(x_i)$ is the Gibbs energy of the disordered solution, which has the same mathematical expression as for a substitutional solution. $G_m^{ord}(y_i', y_i'')$ is the Gibbs energy of the $L1_2$ ordered phase described by a two sublattice model and contains implicitly the contribution from the disordered state. y_i' is the site fraction of Ge and Ni in the first sublattice, and y_i'' in the second one. y_i', y_i'' have the following relation with the mole fraction of component i:

$$x_i = 0.75y_i' + 0.25y_i'' \quad (11)$$

$G_m^{ord}(x_i, x_i)$ represents the energy contribution of the disordered state to the ordered phase. When the site fractions are equal, i.e., $y_i' = y_i''$, the last two terms in Eq. (10) cancel each other, and G_m corresponds to the Gibbs energy of the disordered phase.

The expression of $G_m^{ord}(y_i', y_i'')$, which is given in the form of a two-sublattice model is as follows:

$$\begin{aligned} G_m^{ord}(y_i', y_i'') = {} & y_{Ge}', y_{Ge}''\,^{0}G_{Ge:Ge}^{ord} + y_{Ge}', y_{Ni}''\,^{0}G_{Ge:Ni}^{ord} \\ & + y_{Ni}', y_{Ge}''\,^{0}G_{Ni:Ge}^{ord} + y_{Ni}', y_{Ni}''\,^{0}G_{Ni:Ni}^{ord} \\ & + RT[0.75(y_{Ge}'\ln y_{Ge}' + y_{Ni}'\ln y_{Ni}') \\ & + 0.25(y_{Ge}''\ln y_{Ge}'' + y_{Ni}''\ln y_{Ni}'')] \\ & + y_{Ge}'y_{Ni}'(y_{Ge}''L_{Ge,Ni:Ge}^{ord} + y_{Ni}''L_{Ge,Ni:Ni}^{ord}) \\ & + y_{Ge}''y_{Ni}''(y_{Ge}'L_{Ge:Ge,Ni}^{ord} + y_{Ni}'L_{Ni:Ge,Ni}^{ord}) \end{aligned} \quad (12)$$

In order to favor the stability of the disordered state in certain temperature and composition ranges, G_m should always be a minimum when $y_i' = y_i'' = x_i$ at a certain temperature. Supposing $u_1 = C_1 + D_1T$, $u_2 = C_2 + D_2T$, the following constraints between thermodynamic parameters can be obtained:

$$^{0}G_{Ge:Ni}^{ord} - 0.75\,^{0}G_{Ge}^{disord} - 0.25\,^{0}G_{Ni}^{disord} = 3u_1$$

$$^{0}G_{Ni:Ge}^{ord} - 0.75\,^{0}G_{Ni}^{disord} - 0.25\,^{0}G_{Ge}^{disord} = 3u_1$$

$$^{0}L_{Ge,Ni:Ge}^{ord} = 6u_1$$

$$^{0}L_{Ge,Ni:Ni}^{ord} = 6u_1$$

$$^{1}L_{Ge,Ni:Ge}^{ord} = 3u_2$$

$$^{1}L_{Ge,Ni:Ni}^{ord} = 3u_2$$

$$^{1}L_{Ge:Ge,Ni}^{ord} = u_2$$

$$^{1}L_{Ni:Ge,Ni}^{ord} = u_2$$

The four coefficients, C_1, D_1, C_2 and D_2 are to be optimized in the present work.

4.4. B8-type nonstoichiometric compounds εNi_5Ge_3, $Ni_{19}Ge_{12}$ and Ni_3Ge_2

Since εNi_5Ge_3, $Ni_{19}Ge_{12}$ and Ni_3Ge_2 all have the $B8$-type structure but with some difference in their superstructure [14,21] and they lie next to each other in the phase diagram with less than 1 at% between them [14], they were treated as a single phase in the present optimization and designated as Ni_5Ge_3 to represent the whole $B8$ homogeneity range.

The Ge atoms form an essentially hexagonal close-packed (HCP_A3) array with Ni atoms lying in the octahedral and trigonal bipyramidal interstitial sites. Therefore, a three sublattice model

(Ge)(Ni)(Va,Ni) was used to describe the Ni_5Ge_3 phase consistent with its crystal structure. The first sublattice represents the close packed hexagonal array of the Ge atoms without any substitutions. The second sublattice represents the octahedral positions and is assumed to be completely filled with Ni atoms forming a hexagonal primitive arrangement. The third sublattice contains the trigonal-bipyramidal interstices with some interstitial Ni atoms.

The Gibbs energy of the Ni_5Ge_3 phase is expressed as:

$$G_m^{Ni_5Ge_3} = y_{Va}^{III}\,{}^0G_{Ge:Ni:Va}^{Ni_5Ge_3} + y_{Ni}^{III}\,{}^0G_{Ge:Ni:Ni}^{Ni_5Ge_3} + RT(y_{Ni}^{III}\ln y_{Ni}^{III} + y_{Va}^{III}\ln y_{Va}^{III}) + {}^EG_m^{Ni_5Ge_3}$$

$${}^0G_{Ge:Ni:Va}^{Ni_5Ge_3} = {}^0G_{Ge}^{DIAMOND\_A4} + {}^0G_{Ni}^{FCC\_A1} + E + FT$$

$${}^0G_{Ge:Ni:Ni}^{Ni_5Ge_3} = {}^0G_{Ge}^{DIAMOND\_A4} + 2\,{}^0G_{Ni}^{FCC\_A1} + E' + F'T$$

$${}^EG_m^{Ni_5Ge_3} = y_{Va}^{III}y_{Ni}^{III}L_{Ge:Ni:Va,Ni}^{Ni_5Ge_3}$$

$$L_{Ge:Ni:Va,Ni}^{Ni_5Ge_3} = \sum_{n=0}(G_n + H_nT)(y_{Ni}^{III} - y_{Va}^{III})^n \tag{13}$$

where y_i^{III} is the site fraction of i (i=Va or Ni) in the third sublattice. ${}^0G_{Ge:Ni:Va}^{Ni_5Ge_3}$ and ${}^0G_{Ge:Ni:Ni}^{Ni_5Ge_3}$ are the Gibbs free energy of the corresponding hypothetical end member compounds.

Table 2
Thermodynamic parameters of the Ge-Ni binary system.[a]

Phase	Thermodynamic parameters
Liquid: $(Ge,Ni)_1$	${}^0L_{Ge,Ni}^{Liquid} = -167121.320 + 155T - 15T\ln T$ ${}^1L_{Ge,Ni}^{Liquid} = 84737.489 - 25.014T$ ${}^2L_{Ge,Ni}^{Liquid} = 37441.590 - 16.001T$ ${}^3L_{Ge,Ni}^{Liquid} = -63650.323 + 21.983T$
FCC_A1[b]: $(Ge,Ni)_1$	${}^0L_{Ge,Ni}^{FCC\_A1} = -122000 + 36.88T$ ${}^1L_{Ge,Ni}^{FCC\_A1} = 134000 - 46.8T$ ${}^0Tc_{Ge,Ni}^{FCC\_A1} = -3750$
βNi_3Ge[b]: $(Ge,Ni)_{0.75}(Ge,Ni)_{0.25}$	${}^0G_{Ge:Ni}^{\beta Ni_3Ge} - 0.75\,{}^0G_{Ge}^{DIAMOND\_A4} - 0.25\,{}^0G_{Ni}^{FCC\_A1} = -46827.192 + 3.05T$ ${}^0G_{Ni:Ge}^{\beta Ni_3Ge} - 0.25\,{}^0G_{Ge}^{DIAMOND\_A4} - 0.75\,{}^0G_{Ni}^{FCC\_A1} = -46827.192 + 3.05T$ ${}^0G_{Ge:Ge}^{\beta Ni_3Ge} - {}^0G_{Ge}^{DIAMOND\_A4} = 0$ ${}^0G_{Ni:Ni}^{\beta Ni_3Ge} - {}^0G_{Ni}^{FCC\_A1} = 0$ ${}^0L_{Ge,Ni:Ge}^{\beta Ni_3Ge} = -93654.384 + 6.1T$ ${}^0L_{Ge,Ni:Ni}^{\beta Ni_3Ge} = -93654.384 + 6.1T$ ${}^1L_{Ge,Ni:Ge}^{\beta Ni_3Ge} = 23700 - 9.72T$ ${}^1L_{Ge,Ni:Ni}^{\beta Ni_3Ge} = 23700 - 9.72T$ ${}^0L_{Ni:Ge,Ni}^{\beta Ni_3Ge} = 0$ ${}^0L_{Ni:GeGe}^{\beta Ni_3Ge} = 0$ ${}^1L_{Ni:Ge,Ni}^{\beta Ni_3Ge} = 7900 - 3.24T$ ${}^1L_{Ge:Ge,Ni}^{\beta Ni_3Ge} = 7900 - 3.24T$
γNi_3Ge: $(Ge)_{0.256}(Ni)_{0.744}$	${}^0G_{Ni:Ge}^{\gamma Ni_3Ge} - 0.256\,{}^0G_{Ge}^{DIAMOND\_A4} - 0.744\,{}^0G_{Ni}^{FCC\_A1} = -34315 + 4.301T$
δNi_5Ge_2: $(Ge)_{0.28}(Ni)_{0.72}$	${}^0G_{Ni:Ge}^{\delta Ni_5Ge_2} - 0.28\,{}^0G_{Ge}^{DIAMOND\_A4} - 0.72\,{}^0G_{Ni}^{FCC\_A1} = -34918 + 3.69T$
Ni_2Ge: $(Ge)_{0.335}(Ni)_{0.665}$	${}^0G_{Ni:Ge}^{Ni_2Ge} - 0.335\,{}^0G_{Ge}^{DIAMOND\_A4} - 0.665\,{}^0G_{Ni}^{FCC\_A1} = -38227.151 + 4.849T$
Ni_5Ge_3: (Ge)(Ni)(Va,Ni)[c]	${}^0G_{Ge:Ni:Va}^{Ni_5Ge_3} - {}^0G_{Ge}^{DIAMOND\_A4} - {}^0G_{Ni}^{FCC\_A1} = -54286.304 - 5.624T$ ${}^0G_{Ge:Ni:Ni}^{Ni_5Ge_3} - {}^0G_{Ge}^{DIAMOND\_A4} - 2\,{}^0G_{Ni}^{FCC\_A1} = -110540 + 11.717T$ ${}^0L_{Ge:Ni:Ni,Va}^{Ni_5Ge_3} = -2655.913 - 2.932T$ ${}^1L_{Ge:Ni:Ni,Va}^{Ni_5Ge_3} = -17558.144$
$\varepsilon' Ni_5Ge_3$: $(Ge)_{0.375}(Ni)_{0.625}$	${}^0G_{Ni:Ge}^{\varepsilon' Ni_5Ge_3} - 0.375\,{}^0G_{Ge}^{DIAMOND\_A4} - 0.625\,{}^0G_{Ni}^{FCC\_A1} = -37350.646 + 3.328T$
NiGe: $(Ge)_{0.5}(Ni)_{0.5}$	${}^0G_{Ni:Ge}^{NiGe} - 0.5\,{}^0G_{Ge}^{DIAMOND\_A4} - 0.5\,{}^0G_{Ni}^{FCC\_A1} = -30992.547 + 0.967T - 0.1T\ln T + 6.015E{-}05T^2 - 9.471E{-}08T^3 + 2.393E{-}22T^7 - 14960.491T^{-1}$

[a] Gibbs energies are expressed in J/mol. The lattice stabilities were given by Dinsdale [44].
[b] The ordered phase βNi_3Ge with $L1_2$ structure and disordered phase FCC_A1 are modeled as the same phase.
[c] The sublattice model of the Ni_5Ge_3 phase is given as integral stoichiometry since 1/3 cannot be exactly expressed as a decimal.

$L^{Ni_5Ge_3}_{Ge:Ni:Va,Ni}$ is the interaction parameter between Ni and Va. The parameters E, F, E', F', G_n and H_n are to be optimized.

4.5. Stoichiometric intermetallic compounds

In this work, γNi$_3$Ge, δNi$_5$Ge$_2$, Ni$_2$Ge and NiGe were treated as stoichiometric compounds because little or no homogeneity range was shown for these phases. Since the heat capacity of NiGe was determined by Perring et al. [39], the molar Gibbs energy of NiGe (unit: J/mol) can be expressed as:

$$G_m^{NiGe} = 0.5{}^0G_{Ni}^{FCC\_A1} + 0.5{}^0G_{Ge}^{DIAMOND\_A4} + a + bT + cT\ln T + dT^2 + eT^3 + fT^{-1} + gT^7 \quad (14)$$

where a to g are parameters to be optimized.

Owing to a lack of heat capacity information for the other three intermetallic compounds (γNi$_3$Ge, δNi$_5$Ge$_2$ and Ni$_2$Ge), the Neumann-Kopp rule is applied in order to express their molar Gibbs energies as:

$$G_m^{Ni_xGe_Y} = \frac{x}{x+y}{}^0G_{Ni}^{FCC\_A1} + \frac{y}{x+y}{}^0G_{Ge}^{DIAMOND\_A4} + I_{Ni_xGe_y} + J_{Ni_xGe_y}T \quad (15)$$

where $I_{Ni_xGe_y}$ and $J_{Ni_xGe_y}$ are parameters to be optimized in the present work.

5. Results and discussion

The optimization of the model parameters was conducted using the PARROT module [51] in the Thermo-calc software package developed by Sundman et al. [50].

Table 2 summarizes the optimized thermodynamic parameters for all condensed phases in the Ge-Ni binary system obtained in the present work. The calculated temperatures and compositions of all invariant reactions are compared with the experimental data and those from the previous assessment [10] and listed in Table 3.

Fig. 4 shows the Ge-Ni phase diagram calculated using the optimized parameters produced in the present work. A comparison of the present calculated phase diagram with experimental data is given in Fig. 5. Fig. 5(b) shows an enlarged part of the diagram concerning γNi$_3$Ge and δNi$_5$Ge$_2$, two high temperature phases. As can be seen, reasonable agreement has been obtained between the calculated phase diagram and experimental data. The temperature deviations of the invariant reactions between calculations and experiments are within 6 K. Only the calculated temperature of the eutectic reaction L↔δNi$_5$Ge$_2$+Ni$_5$Ge$_3$ is 7 K higher than the corresponding measured values from Dayer et al. [13]. However, the calculation is still within experimental uncertainties. Only two samples were used to determine the temperature of this eutectic reaction [13]. Besides, it can be seen from Fig. 5 (b) that the temperature intervals between the reactions δNi$_5$Ge$_2$↔βNi$_3$Ge+Ni$_5$Ge$_3$, L↔δNi$_5$Ge$_2$+Ni$_5$Ge$_3$ and the liquidus temperatures

Table 3
Invariant reactions in the Ge-Ni binary system.

Reaction type	Reaction	T/K	Composition (at.% Ge)			Reference
Eutectic	L↔(Ni)+ βNi$_3$Ge	1398	22.8	13.9	23.1	This work
		1397	23.0	~16.0	23.3	[13]
		1399	23.2	15.9	23.3	[10]
Congruent	L↔βNi$_3$Ge	1399	24.0	–	–	This work
		1405	24.0	–	–	[13]
		1399	23.3	–	–	[10]
Peritectic	L+ βNi$_3$Ge↔γNi$_3$Ge	1391	27.3	25.1	25.6	This work
		1391	27.3	~25.0	~25.6	[13]
		1418	–	–	–	[14]
		1428	–	–	–	[12]
		1389	26.7	24.4	25.6	[10]
Peritectic	L+γNi$_3$Ge↔δNi$_5$Ge$_2$	1380	29.1	25.6	28.0	This work
		1375	28.9	25.6	28.0	[13]
		1382	28.0	25.6	28.0	[10]
Eutectoid	γNi$_3$Ge↔βNi$_3$Ge+δNi$_5$Ge$_2$	1355	25.6	25.5	28.0	This work
		1355	25.6	~25.0	28.0	[13]
		1379	–	–	–	[14]
		1357	25.6	24.6	28.0	[10]
Eutectoid	δNi$_5$Ge$_2$↔βNi$_3$Ge+Ni$_5$Ge$_3$	1318	28.0	25.6	35.7	This work
		1318	28.0	25.0	33.6	[13]
		1348	–	–	–	[14]
		1318	28.0	24.7	34.4	[10]
Eutectic	L↔δNi$_5$Ge$_2$+Ni$_5$Ge$_3$	1379	29.2	28.0	35.8	This work
		1372	29.0	28.0	33.6	[13]
		1381	28.4	28.0	34.6	[10]
Peritectoid	βNi$_3$Ge+Ni$_5$Ge$_3$↔Ni$_2$Ge	779	25.5	34.9	33.5	This work
		779	25.0	33.9	33.5	[14]
		779	25.0	33.9	33.5	[10]
Eutectoid	Ni$_5$Ge$_3$↔Ni$_2$Ge+ε′Ni$_5$Ge$_3$	562	35.6	33.5	37.5	This work
		563	36.3	33.5	37.0	[14]
		565	35.2	33.5	37.0	[10]
Congruent	Ni$_5$Ge$_3$↔ε′Ni$_5$Ge$_3$	667	–	37.5	–	This work
		671	–	37.4	–	[14]
		671	–	37.0	–	[10]
Congruent	L↔Ni$_5$Ge$_3$	1453	–	37.3	–	This work
		1458	–	36.5	–	[13]
		1459	–	37.1	–	[10]
Peritectic	εNi$_5$Ge$_3$+L↔NiGe	1129	44.7	57.0	50.0	This work
		1123	~45.0	54.5	50.0	[13]
		1130	44.1	56.8	50.0	[10]
Eutectoid	Ni$_5$Ge$_3$↔ε′Ni$_5$Ge$_3$+NiGe	659	38.2	37.5	50.0	This work
		655	38.2	~37.6	50.0	[14]
		656	38.7	37.0	50.0	[10]
Eutectic	L↔NiGe+(Ge)	1032	65.9	50.0	100	This work
		1035	67.0	50.0	100	[13]
		1048	–	–	–	[12]
		1035	67.4	50.0	100	[10]

for both of those two samples are very narrow (~50 K or even less). Hence, the experimental results of those two samples coming from DTA measurement are rather uncertain.

From Fig. 5(a), it can be seen that the calculated Ni-rich liquidus is a little lower than the experimentally determined line [13]. This could be due to Ge being a moderately volatile element, leading to an error in the actual alloy compositions, containing less Ge than the nominal alloy compositions. The same phenomenon has been observed in the assessments of some other similar systems, such as Ni-Si [52], Ni-Sn [53], Ni-Sb [54] and Ni-Ga [55]. Moreover, the calculated phase boundary of L/L+Ni_5Ge_3 shifts a little to the Ge-rich side compared to the experimental measurement [12,13], which also results in a calculated composition of the liquid (57 at% Ge) of the peritectic reaction L+Ni_5Ge_3↔NiGe deviating from the experimental data (54.5 at% Ge). One possible reason is that εNi_5Ge_3, $Ni_{19}Ge_{12}$ and Ni_3Ge_2 are treated as one phase Ni_5Ge_3 in the present work, thus the ordering effect between εNi_5Ge_3, $Ni_{19}Ge_{12}$ and Ni_3Ge_2 is not considered. An improved thermodynamic model which takes into account the ordering effect between these three *B8*-type phases may improve the calculated liquidus here. However, such a model is not yet available. Another possible reason for the deviation here might be the inconsistency of the experimental data from different literature. The current optimization is based on the evaluated Ge-Ni phase diagram by Nash et al. [15], where the L/L+Ni_5Ge_3 phase boundary and the temperature of the invariant reaction L+Ni_5Ge_3↔NiGe are taken from Dayer et al. [13] while the homogeneity range of εNi_5Ge_3, $Ni_{19}Ge_{12}$ and Ni_3Ge_2 are taken from Ellner et al. [14] since Ref. [12] and Ref. [13] did not confirm the existence of $Ni_{19}Ge_{12}$ and Ni_3Ge_2. It should be noted that the temperatures of the liquidus and the invariant reaction L+Ni_5Ge_3↔NiGe measured by Ellner et al. [14] are much higher than the values measured by Dayer et al. [13].

The calculated solubilities of Ge in (Ni) are in reasonable agreement with the experimental results [13,17,18,19,22]. The maximum solubility of Ge in (Ni) is calculated to be 13.9 at% Ge at 1398 K, while the data reported by Dayer et al. [13] was approximately 16 at% Ge at 1397 K. The current calculation is still acceptable since the maximum solubility of Ge in (Ni) reported by Dayer et al. [13] was the result of extrapolation where large uncertainties may exist. The calculated composition range of Ni_5Ge_3 at the Ni-rich side shifts slightly towards the Ge-rich side. This is the compromise result of keeping the reaction type of L↔δNi_5Ge_2+Ni_5Ge_3 to be eutectic and meanwhile reproducing the temperature of L↔δNi_5Ge_2+Ni_5Ge_3.

The Curie temperature of the FCC_A1(Ni) is well reproduced, as shown in Fig. 5.

Fig. 6 shows the calculated enthalpy of mixing of liquid Ge-Ni alloys at 1288 K, 1773 K and 1870 K, respectively. Good agreement has been obtained at 1773 K between calculation and experiment [26,28]. The enthalpy of mixing of liquid alloys at 1288 K is well reproduced except for the one at 45 at% Ge. It should be noted that Liquid and Ni_5Ge_3 coexist at 45 at% Ge and 1288 K, which will lead to an error in the measurement at this composition. The calculated enthalpies of mixing of the liquid at 1870 K are much more exothermic than the values reported by Erdélyi et al. [29] obtained through indirect measurement. As mentioned in Section 2.2, the indirect method may yield large uncertainties.

The calculated partial enthalpy of mixing of Ni and Ge in Ge-Ni melts at 1800 K compared with experimental data [26,28,30] is shown in Fig. 7. Fig. 8 presents the calculated activity of Ni and Ge in Ge-Ni melts at 1870 K compared with experimental data [27,29,31]. As can be seen, the calculations agree well with the most reliable experimental data as stated in Section 2.2. Fig. 9 shows the

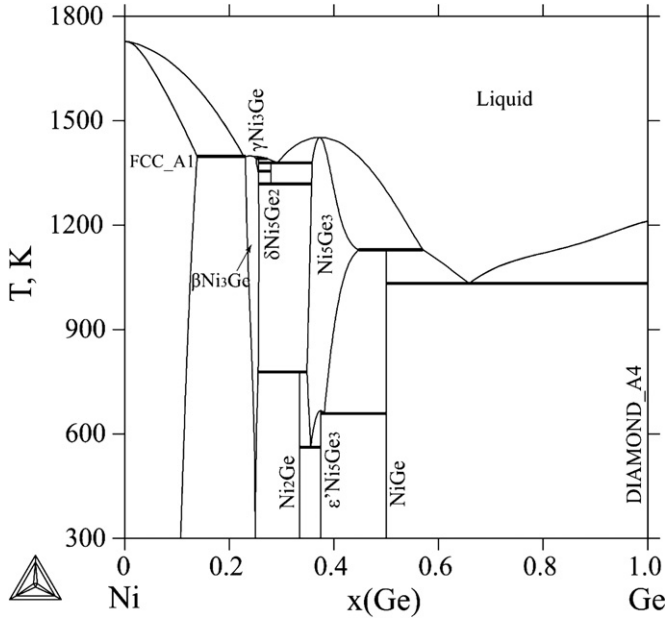

Fig. 4. Calculated phase diagram of the Ge-Ni binary system from the present work.

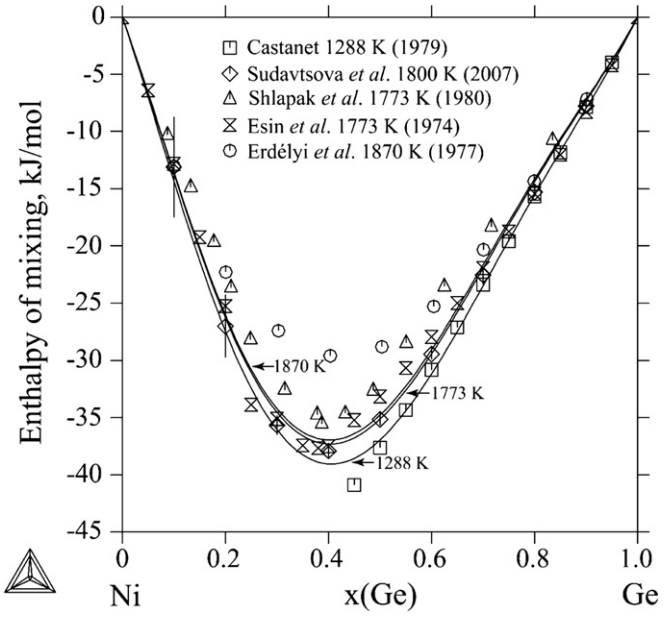

Fig. 6. Calculated enthalpy of mixing of liquid alloys compared with experimental data. (Ref. states: liquid Ge and liquid Ni).

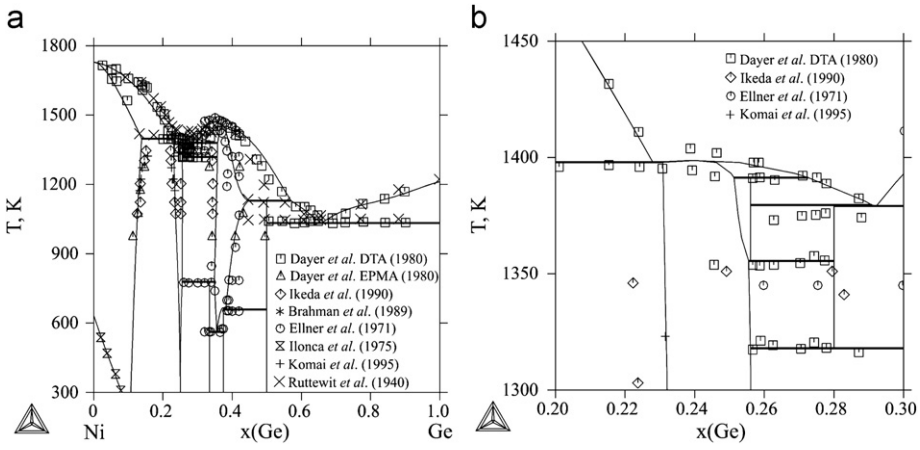

Fig. 5. (a) Calculated phase diagram of the Ge-Ni binary system compared with experimental data. (b) Ni-rich part of the phase diagram compared with experimental data.

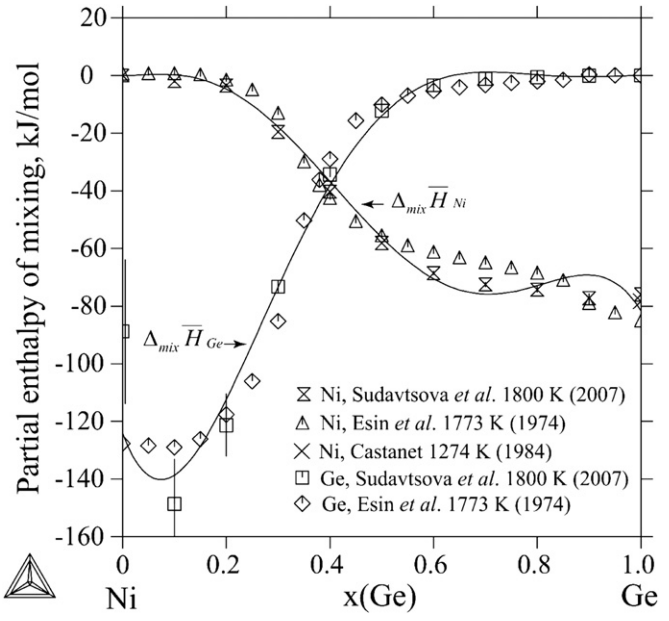

Fig. 7. Calculated partial enthalpy of Ni and Ge in liquid alloys at 1800 K compared with experimental data. (Ref. states: liquid Ge and liquid Ni).

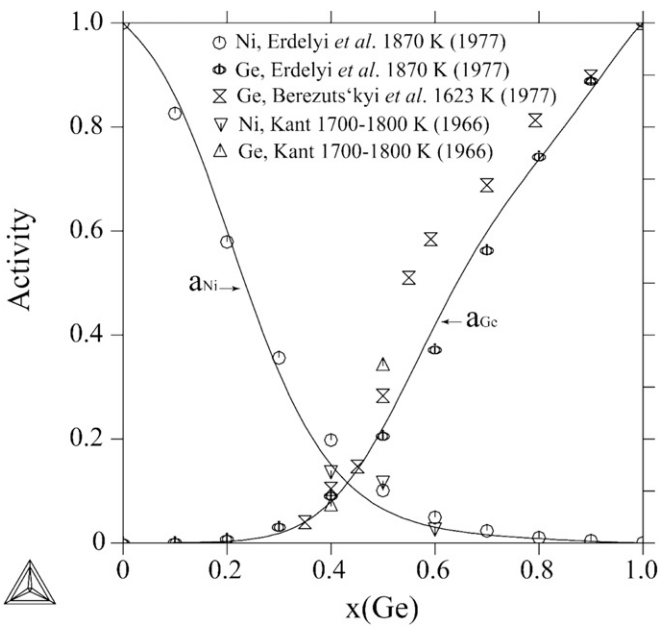

Fig. 8. Calculated activity of Ge and Ni in the Ge-Ni melt at 1870 K compared with experimental data. (Ref. states: liquid Ge and liquid Ni).

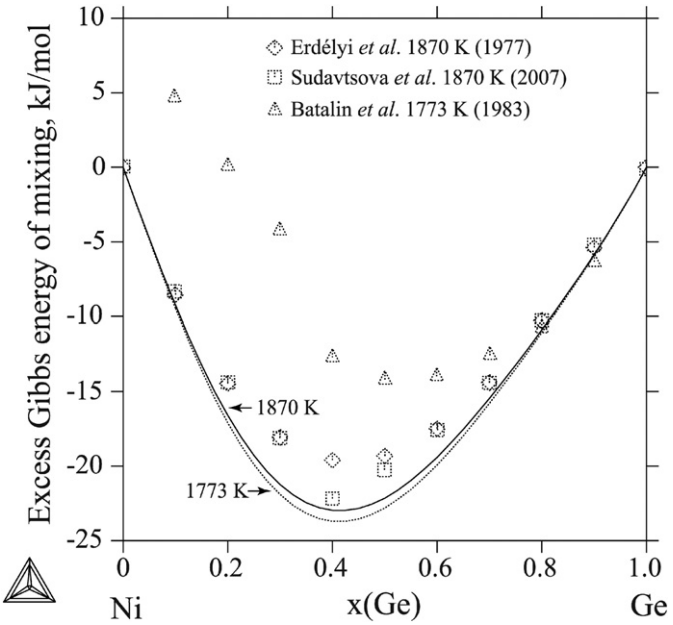

Fig. 9. Calculated excess Gibbs energy of mixing of liquid alloys compared with experimental data. (Ref. states: liquid Ge and liquid Ni).

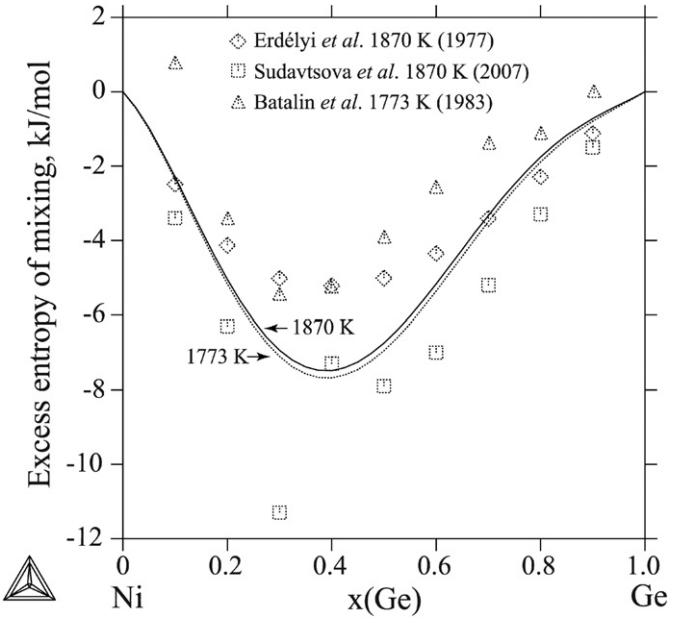

Fig. 10. Calculated excess entropy of mixing of liquid alloys compared with experimental data. (Ref. states: liquid Ge and liquid Ni).

calculated excess Gibbs energies of mixing of Ge-Ni melts. The calculated excess Gibbs energies of mixing are consistent with the reported data from [28,29] while they deviate largely from the data presented in [34] in the composition range 0 to 60 at% Ge. The data from [34] were calculated using the Kubaschewski-Chart equation [36], phase equilibrium data [35] and experimental data on enthalpies of mixing from Shlapak et al. [25]. It should be noted that the Kubaschewski-Chart equation is valid in the region where a pure solid component is in equilibrium with a liquid solution, which corresponds to $0.67 < x_{Ge} < 1$ in the Ge-Ni phase diagram. The calculated minimum of $\Delta_{mix}G_E$ at approximately 40 at% Ge agrees well with the data reported in [28,29]. The calculated excess entropies of mixing of Ge-Ni melts at 1870 K and 1773 K compared with the reported data from literature [28,29,34] are presented in Fig. 10. Reasonable agreement has been obtained while differences were found at the composition of $x_{Ge}=0.1$ compared to [34] and $x_{Ge}=0.3$ compared to [28]. As mentioned above, the data from [34] were calculated by the Kubaschewski-Chart equation, which is valid only from $0.67 < x_{Ge} < 1$. The excess entropy of mixing at $x_{Ge}=0.3$ reported by [28] seems unreliable because it is much more negative compared to all the other values, which will lead to an unreasonable shape of the $\Delta_{mix}S_E$ curve if the excess entropy of mixing data at $x_{Ge}=0.3$ is considered. Therefore, reasonable agreement has been obtained between the calculated excess entropies of mixing and the reported data. Besides, the calculated $\Delta_{mix}S_E$ is negative over the entire composition range, which is consistent with many other transition/non-transition alloy systems.

The calculated enthalpies of formation of solid alloys in the Ge-Ni system at 298 K and 1063 K are shown in Fig. 11. Experimental data from the literature and the calorimetric measurement of the present work, in addition to the results of the first-principles calculations also from this work are superimposed for comparison. As can be seen, the enthalpy of formation of the solid alloys, obtained by the first first-principles and calorimetric measurement in the present work, are more exothermic than the values reported in the literature [8,9,40] except [41]. The difference between the $\Delta_f H$ values calculated from first-principles calculations and those measured by calorimetric measurement in the present work are within ± 5 kJ/mol. But the most exothermic value given by calorimetry is at 36 at% Ge while from first-principles calculations, it is at 50 at% Ge. The difference may arise from a temperature dependence in the enthalpy varying with respect to

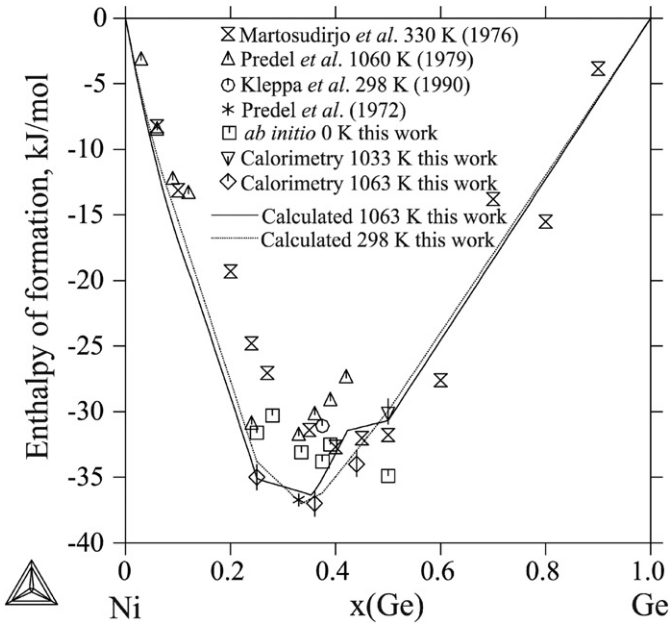

Fig. 11. Calculated enthalpy of formation of solid alloys and intermetallic compounds at 298 K and 1063 K compared with experimental data and *ab initio* data. (Ref. states: 298 K DIAMOND_A4 Ge and ferromagnetic FCC_A1 Ni; 1063 K DIAMOND_A4 Ge and paramagnetic FCC_A1 Ni).

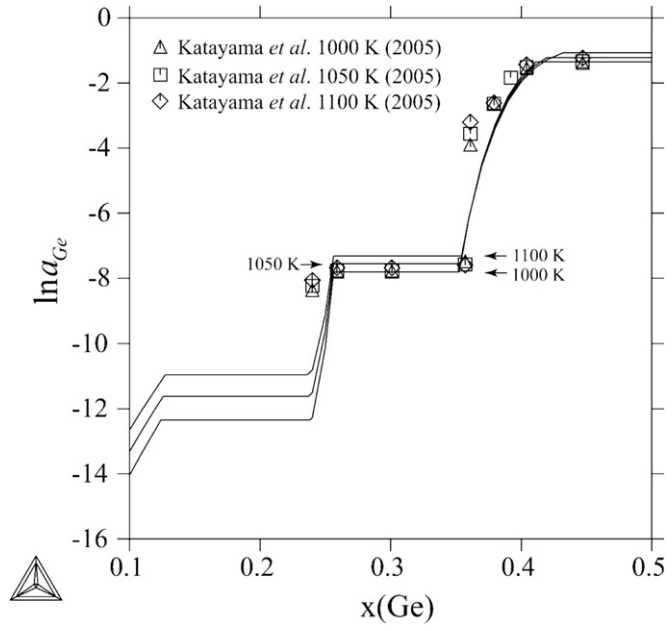

Fig. 12. Calculated activity of Ge in solid alloys at 1000 K, 1050 K and 1100 K compared with experimental data. (Ref. states: DIAMOND_A4 Ge).

composition, bearing in mind that the *ab initio* calculations are performed for 0 K. It may also connected with different reference states, that is, Ni is ferromagnetic at 0 K while it is paramagnetic at the temperatures (1063 K for βNi_3Ge and Ni_5Ge_3, 1033 K for NiGe) that calorimetry was performed.

The enthalpies of formation calculated using the currently optimized parameters agree well with those from calorimetric measurements, whose uncertainty limits are estimated to be only $\pm$(0.3–0.5) kJ/mol, as stated in Section 3.2.1. However, the assessed enthalpy of formation of the Ni_5Ge_3 phase at a composition of 44 at% Ge and T=1063 K is less exothermic than the calorimetric result. Moreover, the experimental phase diagram data could not be well reproduced if a more negative assessed value for the enthalpy of formation was given. The implication is that the Ni_5Ge_3 phase at 44 at% Ge is entropy stabilized in the assessment but this does not explain the disparity with the experiment. This

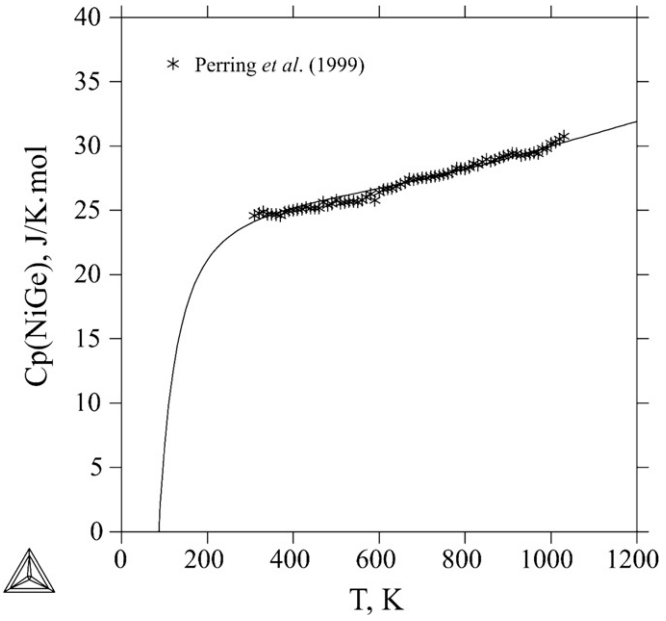

Fig. 13. Calculated heat capacity of NiGe compared with experimental data.

suggests that either this particular experimental measurement has some unknown error or that the modeling of this phase is not appropriate; maybe the simplification used in having a single model for the three *B*8-type phases is not sufficient to describe all of the experimental data in this region. The most exothermic value of the assessed curve appears at around 36 at% Ge, as has been confirmed experimentally in the present work.

The calculated activity of Ge in solid Ge-Ni alloys is shown on a logarithmic scale for 1000, 1050 and 1100 K in Fig. 12. Good agreement has been obtained. Satisfactory reproduction of the experimental heat capacity data of NiGe by the corresponding modeled Gibbs energy is demonstrated in Fig. 13.

6. Conclusions

By a combined CALPHAD, calorimetry and first-principles approach, the thermodynamic functions of the individual phases in the Ge-Ni binary system have been derived. The main results are summarized as follows:

(1) Direct reaction calorimetry has been performed to determine the enthalpies of formation of βNi_3Ge and Ni_5Ge_3 at 1063 K and NiGe at 1033 K.
(2) First-principles calculations have been employed to obtain the enthalpies of formation of βNi_3Ge, δNi_5Ge_2, Ni_2Ge, Ni_5Ge_3 and NiGe compounds and the results are in reasonable agreement with the calorimetric experiments.
(3) The Ge-Ni binary system was re-assessed by incorporating the calorimetry results, first-principles calculations values, critically evaluated literature data and employing appropriate models where crystal structure information was available. A set of self-consistent thermodynamic parameters has been obtained. Most of the experimental data, including phase diagram data and thermodynamic properties, can be accurately described by the present modeling.

Acknowledgment

This work was financially supported by the Swiss State Secretariat for Education and Research (SBF No. C08.0031) within the European COST Action MP0602 on high temperature lead-free solder materials.

Appendix A. Supporting information

Supplementary data associated with this article can be found in the online version at http://dx.doi.org/10.1016/j.calphad.2012.03.003.

References

[1] V. Chidambaram, J. Hald, J. Hattel, J. Alloy. Comp. 490 (2010) 170.
[2] F.Q. Lang, H. Yamaguchi, H. Ohashi, H. Sato, J. Electron. Mater. 40 (7) (2011) 1563.
[3] C. Leinenbach, F. Valenza, D. Giuranno, H.R. Elsener, S. Jin, R. Novakovic, J. Electron. Mater. 40 (7) (2011) 1533.
[4] R. Li, H.B. Yao, S.J. Lee, D.Z. Chi, M.B. Yu, G.Q. Lo, D.L. Kwong, Thin Solid Films 504 (2006) 28.
[5] S. Gaudet, C. Detavernier, A.J. Kellock, P. Desjardins, C. Lavoie, J. Vac. Sci. Technol. A 24 (2006) 474.
[6] A.K. Rai, R.S. Bhattacharya, Y.S. Park, Thin Solid Films 114 (1984) 379.
[7] A. Piotrowska, A. Guivarch, G. Pelous, Solid State Electron. 26 (1983) 179.
[8] S. Martosudirjo, J.N. Pratt, Thermochim. Acta 17 (1976) 183.
[9] B. Predel, W. Vogelbein, Thermochim. Acta 30 (1979) 201.
[10] Y.Q. Liu, D.J. Ma, Y. Du, J. Alloy. Comp. 491 (2010) 63.
[11] L. Kaufman, H. Bernstein, Computer Calculation of Phase Diagrams, Academic Press, New York, 1970.
[12] K. Ruttewit, G. Masing, Z. Metallkd 32 (1940) 51.
[13] A. Dayer, P. Feschotte, J. Less-Common Met. 72 (1980) 51.
[14] M. Ellner, T. Goedecke, K. Schubert, J. Less-Common Met. 24 (1971) 23.
[15] A. Nash, P. Nash, Bulletin of Alloy Phase Diagrams 8 (3) (1987) 255.
[16] H. Pfisterer, U.K. Schubert, Z. Metallkd 41 (1950) 358.
[17] P. Lecocq, Ann. Chim. 8 (1963) 85.
[18] T. Ikeda, Y. Nosé, T. Korata, H. Numakura, M. Koiwa, J. Phase Equilib. 20 (6) (1999) 626.
[19] N. Komai, M. Watanabe, Z. Horita, Acta Metall. Mater 43 (1995) 2967.
[20] P.V. Gel'd, E.S. Levin, V.L. Zagryazhskii, V.N. Zamaraev, Inorg. Mater. Eng. Trans. 15 (1979) 14.
[21] A.-K. Larsson, R. Withers, J. Alloy. Comp. 264 (1998) 125.
[22] I. Rama Brahman, A.K. Jena, M.C. Chaturvedi, Scripta Metall. 23 (1989) 1281.
[23] G. Ilonca, Stud Cercet Fiz 27 (10) (1975) 971.
[24] R. Castanet, J. Chem. Thermodyn. 11 (9) (1979) 913.
[25] A.N. Shlapak, E.A. Beloborodova, G.I. Batalin, Ukr. Khim. Zh. 46 (2) (1980) 209.
[26] Yu.O. Esin, V.K. Zavyalov, M.S. Petrushevskii, P.V. Geld, E.S. Levin, Theory and Technology of Metallothermic Processes, Nauka, Novosibirsk, 1974, p. 96.
[27] A. Kant, J. Chem. Phys. 44 (6) (1966) 2450.
[28] V.S. Sudavtsova, N.V. Kotova, T.N. Zinevich, Inorg. Mater 43 (5) (2007) 488.
[29] L. Erdélyi, A. Neckel, J. Tomiska, H. Nowotny, Ber. Bunsen-Ges. Phys. Chem. 81 (10) (1977) 1003.
[30] R. Castanet, J. Less-Common Met. 103 (1984) L1.
[31] V.V. Berezuts'kyi, V.N. Eremenko, G.M. Lukashenko, Dopov. Akad. Nauk. Ukr. RSR, Ser. B: Geol., Khim. Biol. Nauki (1977) 123.
[32] E. Schroeder, Math. Ann. 3 (2) (1870) 296.
[33] V.S. Sudavtsova, Thermodynamics of Metallurgical and Welding Melts. 2. Alloys Based on Silicon and Copper [in Russian], Logos, Kiev (2005) 167.
[34] G.I. Batalin, A.N. Shlapak, Ukr. Khim. Zh. 49 (1) (1983) 11.
[35] M. Hansen, I. Anderko, Structure of Binary Alloys, Metallurgiya, Moscow 2 (1962).
[36] O. Kubaschewski, T.G. Chart, J. Inst. Metals 94 (1965) 329.
[37] L.I. Erokhin, K.P. Gurov, Rasplavy 7 (4) (1993) 3.
[38] I. Katayama, T. Hori, M. Sakai, H. Numakura, T. Iida, Z. Metallkd 96 (2005) 853.
[39] L. Perring, J.J. Kuntz., F. Bussy, J.C. Gachon, Intermetallics 7 (11) (1999) 1235.
[40] O.J. Kleppa, Woo-Gwang Jung, High Temp. Sci. 29 (1990) 109.
[41] B. Predel, H. Ruge, Thermochim. Acta 3 (5) (1972) 411.
[42] S.J. Clark, M.D. Segall, C.J. Pickard, P.J. Hasnip, M.J. Probert, K. Refson, M.C. Payne, Z. Kristallogr. 220(5-6) ((2005) 567.
[43] J.P. Perdew, K. Burke, M. Ernzerhof, Phys. Rev. Lett. 77 (1996) 3865.
[44] G. Cacciamani, G. Borzone, R. Ferro, J. Alloys Compd. 220 (1995) 106.
[45] G. Borzone, R. Raggio, R. Ferro, J. Alloys Compd. 367 (2004) 89.
[46] A.T. Dinsdale, CALPHAD 15 (1991) 317.
[47] O. Redlich, A.T. Kister, Ind. Eng. Chem. 40 (1948) 345.
[48] M. Hillert, M. Jarl, CALPHAD 2 (1978) 227.
[49] I. Ansara, N. Dupin, L.L. Lukas, B. Sundman, J. Alloys Comp. 247 (1997) 20.
[50] B. Sundman, B. Jansson, J.O. Andersson, CALPHAD 9 (1985) 153.
[51] B. Jansson, Tricta-Mac-0234, Royal Institute of Technology, Stockholm, Sweden, 1984.
[52] T. Tokunaga, K. Nishio, H. Ohtani, M. Hasebe, CALPHAD 27 (2003) 161.
[53] H.S. Liu, J. Wang, Z.P. Jin, CALPHAD 28 (2004) 363.
[54] Y.B. Zhang, C.R. Li, Z.M. Du, C.P. Guo, CALPHAD 32 (2008) 378.
[55] W.X. Yuan, Z.Y. Qiao, H. Ipser, G. Eriksson, J. Phase Equilib. Diff. 25 (2004) 68.